Bulletin of Electrical Engineering and Informatics
Vol. 15, No. 1, February 2026, pp. 11~26
ISSN: 2302-9285, DOI: 10.11591/eei.v15i1.10220

Optimized FOI-TD controller for automatic generation control of restructured power systems with sodium-ion batteries

Nanthini B S[1], Ilanji Akilandam Chidambaram[1], Rajeswaran Sivasangari[2]
[1]Department of Electrical Engineering, Annamalai University, Annamalainagar, India
[2]Department of Electrical and Electronics Engineering, Sree Sowdambika College of Engineering, Aruppukkottai, India

Article Info

Article history:

Received Mar 6, 2025
Revised Oct 17, 2025
Accepted Dec 6, 2025

Keywords:

Automatic generation control
Distribution companies
Fractional order integral-tilt derivative controller
Generation companies
Moth flame optimization
Sodium ion batteries

ABSTRACT

This article examines a novel control technique known as the fractional order integral-tilt derivative (FOI-TD) controller, which was used for automatic generation control (AGC) with a two-area restructured power system. The FOI-TD controller enhances performance by integrating tilt-derivative control with fractional-order control. Fractional-order control offers greater flexibility and allows for more precise tuning of the controller's response. The tilt component modifying the proportional term minimizes overshoot and improves settling times. The control parameters of the FOI-TD controller are optimized using the moth flame optimization (MFO) method and the efficacy of the given algorithm is associated with recent studies using meta-heuristic techniques. Analysis indicates that the MFO-optimized FOI-TD controller substantially enhances the dynamic response of the AGC loop and compared with traditional controllers. This enhancement includes reduced peak deviations, shorter settling times, and better suppression of area frequencies and tie-line power oscillations across different transaction scenarios within restructured power system. To further enhance AGC performance, fast-acting energy storage systems, like sodium-ion batteries (SIB), are integrated into the control area. The coordinated operation of the SIB units improves system dynamics and stability by mitigating initial frequency drops and tie-line power variations caused by sudden load disturbances.

Corresponding Author:

Nanthini B S
Department of Electrical Engineering, Annamalai University
Annamalainagar, Tamil Nadu, India
Email: nanthini.b.s.18@gmail.com

1. INTRODUCTION

Automatic generation control (AGC) is a vital component in managing the stability of the power systems. It ensures an appropriate balance among the electricity generation and the constantly fluctuating load demand of electrical network. When there are discrepancies in power supply and demand, it can lead to oscillations in system performance, negatively affecting frequency regulation [1]. Power grids require near-instantaneous balance between generation and load, which necessitates frequent adjustments to generator outputs. The system frequency serves as a key indicator of this balance: a rising frequency indicates an excess of generation, causing the system to accelerate, while a falling frequency signifies insufficient generation, resulting in system deceleration. To restore frequency balance, control actions adjust the load reference position through the speed changer mechanism, ensuring the stability and reliability of the system [1], [2]. The area control error (ACE) is the foundation on which the AGC system operates, taking system frequency and tie-line flows as inputs. AGC calculates the necessary adjustments to power generation based

on changes in demand by monitoring regional frequency and tie-line power flows [3]. To reduce ACE, in an interconnected power system, generator set points are adjusted based on a linear integration of frequency variations and tie-line power exchanges. As the AGC loop operates to drive the ACE toward zero, frequency deviations and tie-line power errors also approach negligible values [4], [5].

In a restructured electricity market, multiple entities interact, including generation companies (Gencos), distribution companies (Discos), transmission companies (Transcos), and independent system operators (ISOs) [6]. The AGC system must manage different types of contracts, such as Poolco arrangements, bilateral agreements, and hybrid contracts. For bilateral transactions, Discos are the flexibility to procure power from any available Genco, both within and outside their region. The conventional AGC system, originally designed for two interconnected zones, has been adapted to account for the impact of these market transactions on system dynamics [7], [8]. Under ISO supervision, each control area is reason for managing its load and adhering to tie-line power agreements. To facilitate these agreements, a disco participation matrix (DPM) is employed, representing contractual relationships between Discos and Gencos [9]–[11]. Each column in the DPM sums to one, indicating the proportion of a Disco's total load allocated to a particular Genco.

To improve dynamic performance, AGC systems commonly employ various control strategies. Conventional controllers, such as proportional-integral (PI) and proportional-integral-derivative (PID) controllers, remain popular by virtue of their simplicity, robustness, ease of implementation, and cost-effectiveness [12], [13]. While PI controllers provide reliable dynamic responses, they may struggle under increasing system complexity or disturbances, leading to steady-state errors [14], [15]. PID controllers, with their derivative component, can enhance stability but may produce noisy or erratic control signals under rapidly changing inputs [16]. First-order filters are often applied to the derivative term to mitigate noise. Advanced controller variations, including proportional-integral-derivative controller with a derivative filter (PIDF) and fractional-order PID controllers, further improve performance under parameter uncertainties [17]–[19]. In this study, a fractional order integral with tilt derivative (FOI-TD) controller is implemented as a secondary controller to enhance the AGC response of a two-area interconnected power system. Its performance is compared against conventional PI and PIDF controllers.

Soft computing-based optimization techniques has been widely applied to improve power system control, including genetic algorithm (GA), particle swarm optimization (PSO), bat algorithm (BAT), bacterial foraging optimization (BFO), differential evolution (DE), and ant lion optimizer (ALO) [1], [20]. The effectiveness of any optimization technique depends on both convergence behavior and the optimal solution obtained. Traditional integral squared error (ISE) methods are often complex, time-consuming, and prone to suboptimal solutions. GA, while powerful, requires evaluating large populations, leading to high computational time and susceptibility to local minima. PSO also exhibits limitations in local search capability, increasing the likelihood of stagnation [21]. The BAT algorithm may stagnate due to rapid changes in loudness and pulse rates during the exploitation phase. Among these, ALO performs efficiently for load frequency control (LFC) problems due to its minimal parameter tuning requirements [22]. Recently, the moth flame optimization (MFO) algorithm has been injected to optimal controller gains and values. Inspired by moth navigation behavior, MFO efficiently improves initial random solutions and converges toward optimal points in the search space [23]–[25].

Energy storage devices, such as batteries, play an important role in AGC by providing rapid and flexible responses to load changes, enhancing frequency regulation and system stability [26]–[28]. Fast-acting energy storage systems (ESS) improve supply reliability by storing electricity during low-peak periods and delivering it during peak demand. With the increasing need for grid stability and growing energy demands, integrating fast-acting battery storage into AGC loops has become crucial. Sodium-ion batteries (SIBs) are emerging as alternative to lithium-ion technology, offering advantages in cost, abundance, and environmental impact [29]–[32]. These batteries use sodium ions (Na^+) instead of lithium ions (Li^+) for energy storage and are suitable for large-scale power system applications. In this study, SIBs are incorporated into the AGC loop of a two-region thermal power system, demonstrating their effectiveness in reducing frequency difference and enhancing system resilience under diverse operating conditions.

2. METHOD

The AGC system functions through two primary feedback mechanisms: the primary control loop and the secondary control loop. The primary loop manages the turbine–governor response to continuous changes in load, allowing the system frequency to stabilize at a new operating point following a disturbance. The secondary loop then restores the frequency to its nominal value by automatically adjusting generator set points through the speed changer mechanism. This process ensures that discrepancies between total generation, power demand, and system losses are corrected effectively [1]–[3]. In this work, a MFO tuned FOI-TD controller is applied to each area of the test network. To further improve AGC performance, the study focuses on strategically utilizing SIBs within the control areas of proposed power system.

2.1. Modelling of two-area restructutred power system

AGC operates with the ACE signal that reflects deviations in system frequency and variations in tie-line power flows. By acting to minimize these deviations, AGC helps in maintain the stability and balance of power system, effectively driving the ACE toward zero [4]. Figure 1 depicts the transfer function approach of a two-region thermal power system under a restructured market framework, comprising Gencos, Transcos, and Discos, each with distinct operational responsibility. In this setup, a Disco in any region can establish contracts with Gencos both within its own region and across other regions. Discos can contract power from any Genco in the deregulated framework, with the ISO coordinating these agreements. These various contracts are managed and showed by the DPM, which shows how much load demand each Disco gives to different Gencos [6], [7].

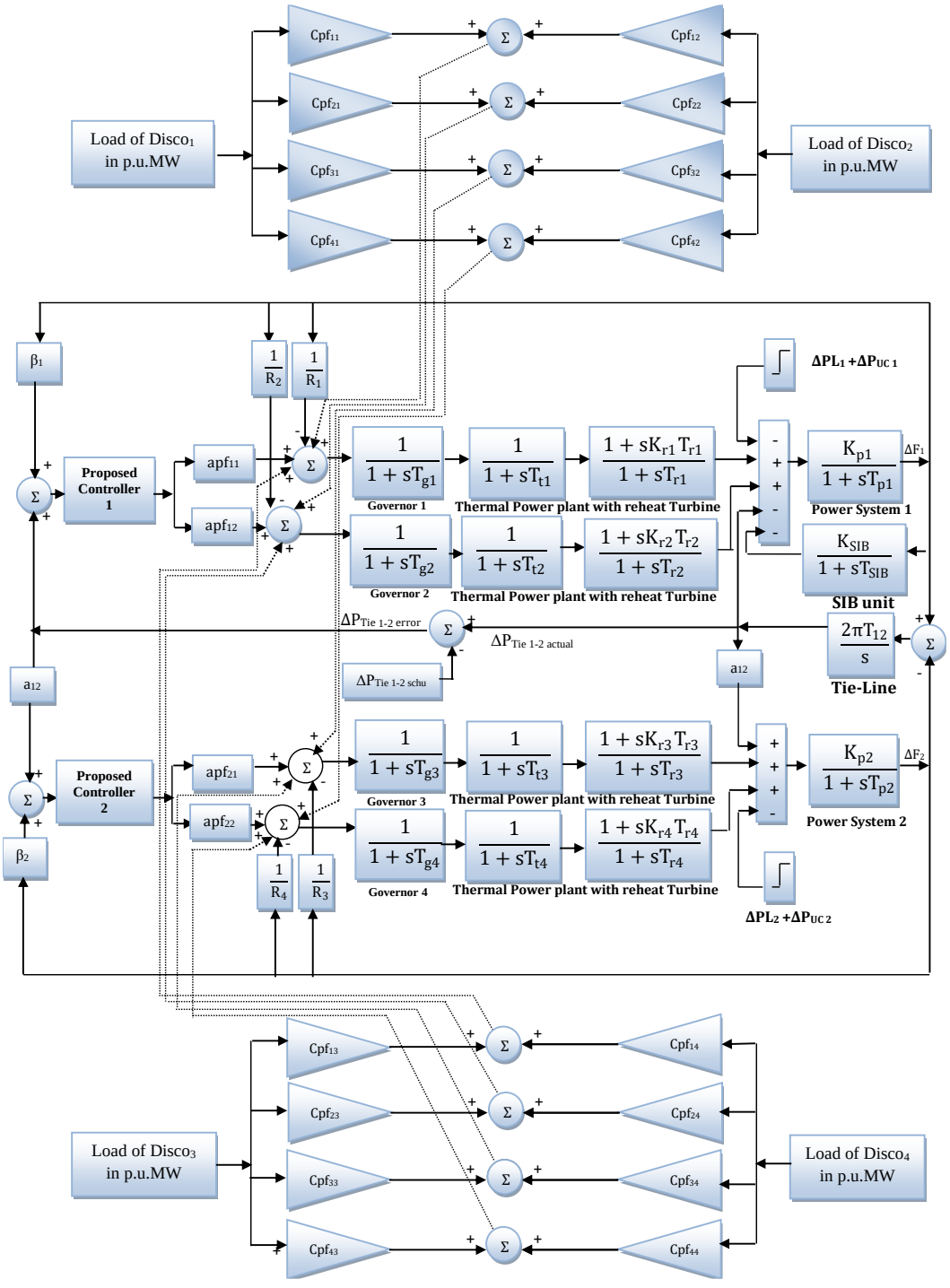

Figure 1. Linearized model of a two-area restructured power system using proposed controller with SIB unit

This study shows a thermally interconnected power system which wascategorised into two areas. Each areahave two Gencos are linked through a DPM, which defines the contractual power exchanges between them. The matrix can be written as (1):

$$DPM_i = \begin{bmatrix} cpf_{11} & cpf_{12} & cpf_{13} & cpf_{14} \\ cpf_{21} & cpf_{22} & cpf_{23} & cpf_{24} \\ cpf_{31} & cpf_{32} & cpf_{33} & cpf_{34} \\ cpf_{41} & cpf_{42} & cpf_{43} & cpf_{44} \end{bmatrix} \quad (1)$$

Here, contract participation factor (CPF) specifies the portion of a Disco's load demand that each Genco must supply. The scheduled power flow on the tie-line between two areas is calculated as (2):

$$\Delta P_{Tie\ 12}^{scheduled} = \sum_{i=1}^{2}\sum_{j=3}^{4} cpf_{ij}\,\Delta P_{Lj} - \sum_{i=3}^{4}\sum_{j=1}^{2} cpf_{ij}\,\Delta P_{Lj} \quad (2)$$

The actual tie-line power flow is given by (3):

$$\Delta P_{Tie\ 12}^{actual} = \frac{2\pi T_{12}}{s}(\Delta F_1 - \Delta F_2) \quad (3)$$

The tie-line power error, i.e., the deviation from the scheduled flow, can be expressed as (4):

$$\Delta P_{Tie\ 12}^{error} = \Delta P_{Tie\ 12}^{actual} - \Delta P_{Tie\ 12}^{scheduled} \quad (4)$$

During steady-state conditions, this error approaches zero as actual power transfer matches the allotted value. The error signal is further used to compute the ACE for each control area as (5) and (6):

$$ACE_1 = \beta_1\,\Delta F_1 + \Delta P_{tie_{12}}^{error} \quad (5)$$

$$ACE_2 = \beta_2\,\Delta F_2 + \alpha_{12}\Delta P_{tie_{12}}^{error} \quad (6)$$

2.2. Controller structure and optimization techniques

Various integer and fractional order controllers are utilized for AGC in different power system applications. In the literature, the PI controllers are widely used and effective for a broad range of automatic AGC applications and the transfer function can be expressed mathematically as (7):

$$TF_{PI}(s) = K_P + \frac{K_I}{s} \quad (7)$$

The main drawback of the PI controller is its inability to predict future errors in the system, which prevents it from eliminating steady-state oscillations and can result in an increase in settling time. As a result, the overall stability of the system is relatively low [12]–[14]. In contrast, the PID controller features a derivative mode that enhances system stability. This mode allows for an increase in proportional gain and a decrease in integral gain, ultimately improving the controller's response speed. However, the derivative term in a control system can lead to excessively large control inputs when the input signal experiences abrupt changes or sharp corners. Additionally, noise present in the input signal can generate significant control signals, complicating practical applications [13]. A viable solution to this problem is to apply a first-order filter to the derivative term, adjusting its pole to reduce high-frequency chattering caused by noise. In that context, a PIDF was explored as a potential solution. FOI-TD controllers enhance performance and adaptability by incorporating fractional orders. In contrast, TID controllers elevate standard PID controllers by introducing a "tilted" behavior instead of relying solely on proportional action. A two-degree-of-freedom (2DOF) PID controller offers advantages such as separate tuning for set point changes and better disturbance rejection. However, FOI-TD controllers take control to an advanced level by utilizing fractional orders, which surpass the discrete integer degrees of freedom found in a 2DOF PID controller, resulting in more sophisticated and robust control actions. The transfer function of the PIDF controller can be expressed as (8):

$$TF_{PIDF}(s) = K_P + \frac{K_I}{s} + K_D\left(\frac{Ns}{s+N}\right) \quad (8)$$

The FOI-TD controller is an advanced control technique that employs fractional calculus to enhance performance, and it is the focus of this study. This controller combines integral and derivative actions with an

additional "tilt" component, which improves damping and robustness in comparison to traditional PI and PIDF controllers. The control configuration of the FOI-TD controller is illustrated in Figure 2.

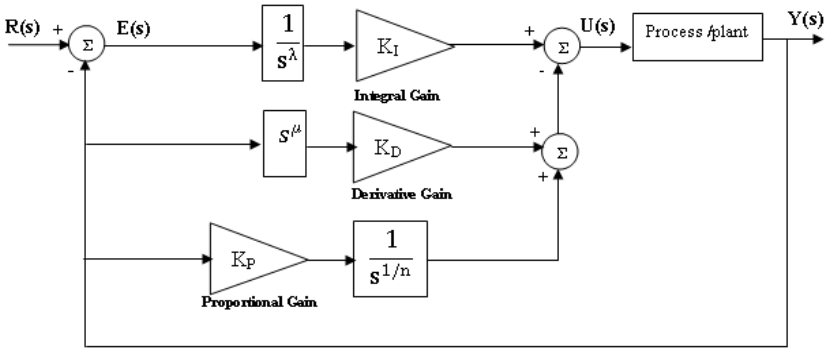

Figure 2. Model of FOI-TD controller

The transfer function of the FOI-TD controller is mathematically represented as (9):

$$TF_{FOI-TD)}(s) = \frac{K_I}{s^{\lambda}} E(s) - Y(s)\left(\frac{K_P}{s^{1/n}} + K_D s^{\mu}\right) \quad (9)$$

In this controller design, K_P, K_I, and K_D denote the proportional, integral, and derivative gains, while λ and μ correspond to the fractional orders of integration and differentiation, respectively. The objective function is formulated according to the defined performance requirements and design constraints, serving as the basis for applying a modern heuristic optimization method to tune the proposed controller. Performance indices—like the integral of squared error (ISE)—are commonly employed to evaluate and enhance control performance, as (10):

$$J_i = \int_0^{t_{sim}} [(ACE_i)^2]\, dt \quad (10)$$

Minimization of J_i must be achieved within the bounds defined by the control parameters of the proposed controllers, subject to:

$$K_P^{min} \le K_P \le K_P^{max}, K_I^{min} \le K_I \le K_I^{max}, K_D^{min} \le K_D \le K_D^{max}, \lambda^{min} \le \lambda \le \lambda^{max}, \mu^{min} \le \mu \le , n^{min} \le n \le n^{max} \quad (11)$$

The MFO algorithm is a nature-motivated metaheuristic optimization technique. It inspires from the navigate method of moths in nature, known as transverse orientation. MFO has been utilized in a vast range of optimization issues across various aspects, including engineering design, image processing, machine learning, and power systems optimization, owing to its simplicity and effectiveness. Additionally, several variants and hybrid versions of MFO have been developed to tackle specific challenges, such as premature convergence and the issue of getting trapped in local optima [23], [24]. In this paper, the given controllers designed with the MFO algorithm are compares with other nature-inspired algorithms, such as PSO, BAT, and ALO [1], [20]–[22]. The proposed controller's lower and upper bounds for the controller gains K_P, K_I, and K_D are 0.01 and 5 respectively and the partial order component λ and μ can be given within the range [0,2].

2.3. Control design for sodium-ion batteries in automatic generation control loop

Figure 3 presents the modeling and integration of a SIB within a restructured power system for AGC applications. The Figure 3 illustrates both the internal structure of the SIB unit and its role in the dynamic behavior of a two-area power system. Figure 3(a) shows the schematic representation of an SIB unit. Following a load disturbance, it is essential to rapidly recharge or restore the SIB capacity to ensure its availability for subsequent disturbances. Owing to their fast dynamic response, SIBs are highly advantageous in AGC applications, as they can minimize action delays. In this setup, the frequency deviation (ΔFi) is explicitly employed as the control input to the AGC system to monitor the SIB's power output. The control actions of SIB systems have been observed to outperform conventional governor systems in terms of

response speed to frequency variations. SIB units are specifically designed to rapidly suppress peak frequency deviations caused by sudden load changes. Once these peak deviations are mitigated, the governor system assumes control to compensate for any remaining steady-state frequency errors. Figure 3(b) presents a linearized reduced-order model of a two-area restructured power system incorporating SIB units.

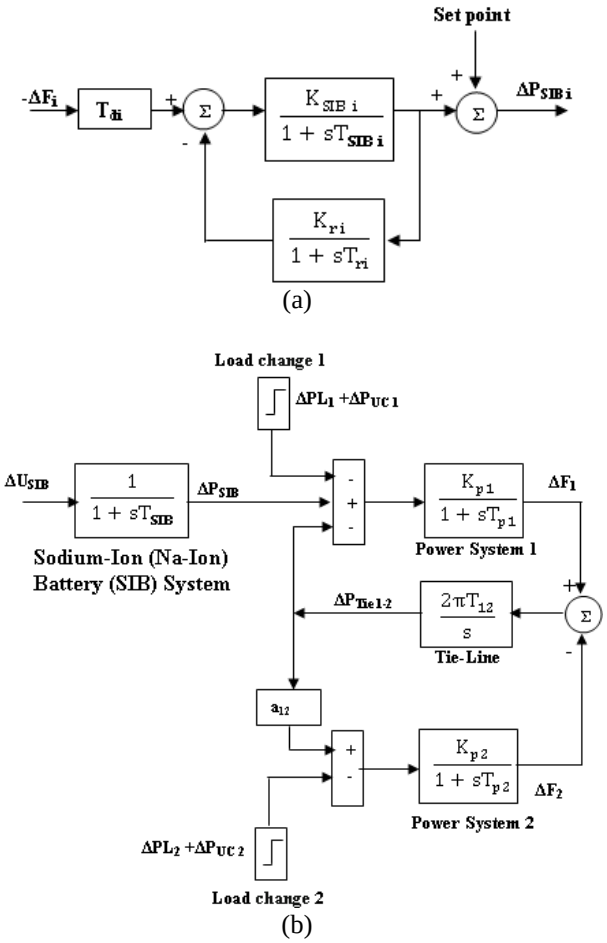

Figure 3. Modeling and integration of a SIB within a restructured power system; (a) schematic representation of an SIB unit and (b) linearized reduced-order model of a two-area restructured power system incorporating SIB unit

In this model, SIB units is depicted as active power source in area 1, defined by a time constant T_{SIB} and a gain constant K_{SIB}. For control design purposes, if we assume the time constant T_{SIB} to be zero, the state equation for the system, as shown in Figure 3(b), simplifies to:

$$\begin{bmatrix} \Delta\dot{F}_1 \\ \Delta\dot{P}_{T12} \\ \Delta\dot{F}_2 \end{bmatrix} = \begin{bmatrix} -1/T_{p1} & -k_{p1}/T_{p1} & 0 \\ 2\pi T_{12} & 0 & -2\pi T_{12} \\ 0 & a_{12}\,k_{p2}/T_{p2} & -1/T_{p2} \end{bmatrix} \begin{bmatrix} \Delta F_1 \\ \Delta P_{T12} \\ \Delta F_2 \end{bmatrix} + \begin{bmatrix} k_{p1}/T_{p1} \\ 0 \\ 0 \end{bmatrix} [\Delta P_{SIB}] \quad (12)$$

To reduce frequency variations at the inertia center, the SIB unit's control design is structured as a single-region system. The derivative of ΔP_{T12} in (10) becomes:

$$\frac{\Delta\dot{P}_{T12}}{2\pi T_{12}} = \Delta F_1 - \Delta F_2 \quad (13)$$

If the synchronizing power coefficient (T_{12}) is infinite, then in (12) becomes $\Delta F_1 = \Delta F_2$. The control gain of the SIB unit is detailed in [33]. The control gain of SIB unit is given as:

$$K_{sib} = (A/BR) * (100 - R) \quad (14)$$

where $A = \left(-1/k_{p1} - (1/a_{12}k_{p2})\right)/\left((T_{p1}/k_{p1}) + (T_{p2}/a_{12}k_{p2})\right)$
$B = 1/\left((T_{p1}/k_{p1}) + (T_{p2}/a_{12}k_{p2})\right)$

3. RESULTS AND DISCUSSION

This study investigates the AGC performance of a two-area thermal restructure power system under two operational scenarios: with and without the integration of SIB units, using a proposed advanced control strategy. Each control area comprises two Gencos and two Discos, where the Gencos are modeled as thermal reheat power plant units. The complete power system model is developed and simulated in the Simulink/MATLAB environment. The key parameter values associated with the two-area thermal plants and the SIB units are presented in Table 1. The controller tuning process is referred as an optimization issue, with the objective functions defined in (10) and (11) aiming to reduce frequency deviations in each control area and mitigate tie-line power deviations. Power transactions among Discos and Gencos are categorized into two types: Poolco-based transactions, which occur when a Disco procures power from a Genco within the same control area, and bilateral transactions, which occur if a Disco enter into a contract with a Genco from a different area. The SIB unit is located in area 1, and its gain value is calculated using in (14) for a specific steady-state speed regulation of the governor. The MFO metaheuristic technique is employed to optimize the gains and control parameters of the proposed controllers, including PI, PIDF, and FOI-TD. These controllers are evaluated individually and compared with the PSO, BAT, and ALO techniques.

Table 1. Parameters of Gencos, control area, and SIB unit [12], [27]

Parameters	Area 1	Area 2
Area capacities (MW)	1000	1000
Rating of Gencos (MW)	500	500
Kp (Hz/p.u.MW)	120	120
Tp (sec)	20	20
β (p.u.MW/Hz)	0.425	0.425
R (Hz/p.u.MW)	$R_1=R_2=2.4$	$R_3=R_4=2.4$
Tg (sec)	$T_{g1}=T_{g2}=0.08$	$T_{g3}=T_{g3}=0.08$
Tt (sec)	$T_{t1}=T_{t2}=0.36$	$T_{t3}=T_{t4}=0.36$
T_r (sec)	$T_{r1}=T_{r2}=10$	$T_{r3}=T_{r4}=10$
K_r	$K_{r1}=K_{r2}=0.5$	$K_{r3}=K_{r4}=0.5$
Area participation factor (apf)	$apf_{11}=apf_{12}=0.5$	$apf_{21}=apf_{22}=0.5$
Synchronising coefficient (p.u.MW/Hz)	$2\pi T_{12}=0.545$	
Area capacity ratios	$a_{12}=-1$	
System frequency (F) in Hz	60 Hz	
Parameters of SIB unit	$T_{SIB}=0.01$ (sec) $T_{di}=0.002$ (sec)	$K_{ri}=1$, $T_{ri}=0.002$ (sec)

3.1. Scenario 1: Poolco-based transactions

In Poolco-based transactions, each Genco supplies power exclusively to the Discos within its own area. For example, the Discos in area 1 have a power demand while the Discos in area 2 do not request any supply, a load varies of 0.2 p.u. MW is assumed to every Disco in area 1. The DPM for Poolco-based transactions is expressed in (15). In this case, $Disco_1$ and $Disco_2$ share power equally from the local $Genco_1$ and $Genco_2$.

$$DPM_1 = \begin{bmatrix} 0.5 & 0.5 & 0.0 & 0.0 \\ 0.5 & 0.5 & 0.0 & 0.0 \\ 0.0 & 0.0 & 0.0 & 0.0 \\ 0.0 & 0.0 & 0.0 & 0.0 \end{bmatrix} \quad (15)$$

The optimal parameter estimations for the proposed controller in the test system have been achieved using PSO, BAT, ALO, and MFO algorithms. The convergence characteristics and control parameters of these controllers were presented in Tables 2 and 3. It is evident from these Tables that the convergence of the MFO algorithm is faster, and the cost function values (J_i) are lower compared to the PSO, BAT, and ALO techniques. Given the convergence and measurable performance of these algorithms, the design of the proposed MFO-based controllers has been implemented for a two-area power system for further analysis.

Table 2. Convergence characteristics of PSO, BAT, ALO, and MFO algorithms

Convergence characteristics	PSO	BAT	ALO	MFO
Average fitness	7.568×10^{-4}	6.265×10^{-4}	5.187×10^{-4}	4.078×10^{-5}
Worst fitness	9.152×10^{-3}	8.214×10^{-3}	7.978×10^{-3}	5.941×10^{-3}
Best fitness	8.978×10^{-5}	7.527×10^{-5}	6.457×10^{-5}	3.143×10^{-5}
Standard deviation	7.896×10^{-3}	5.214×10^{-3}	4.214×10^{-3}	2.478×10^{-3}
Convergence of iteration	65	55	40	30

Table 3. Control parameters of test system using PI, PIDF, and FOI-TD controllers for Poolco transactions

Control	PSO			BAT			ALO			MFO		
parameters	PI	PIDF	FOI-TD	PI	PIDF	FOI-TD	PI	PIDF	FOI-TD	PI	PIDF	FOI-TD
K_{P1}	0.324	0.303	0.241	0.315	0.294	0.232	0.309	0.288	0.207	0.295	0.268	0.202
K_{I1}	0.497	0.571	0.617	0.481	0.592	0.669	0.492	0.597	0.672	0.521	0.647	0.745
K_{D1}	-	0.805	0.843	-	0.826	0.855	-	0.771	0.863	-	0.814	0.897
N_1	-	26.33	-	-	29.78	-	-	30.15	-	-	35.42	-
λ_1	-	-	0.675	-	-	0.621	-	-	0.598	-	-	0.474
μ_1	-	-	0.621	-	-	0.694	-	-	0.704	-	-	0.806
n_1	-	-	0.512	-	-	0.578	-	-	0.589	-	-	0.611
J_1 ($\times10^{-3}$)	117	89	59	108	85	55	97	78	50	62	58	41
K_{P2}	0.315	0.301	0.244	0.309	0.293	0.212	0.294	0.285	0.208	0.218	0.203	0.195
K_{I2}	0.463	0.443	0.532	0.472	0.483	0.572	0.486	0.492	0.585	0.547	0.588	0.691
K_{D2}	-	0.503	0.632	-	0.547	0.656	-	0.553	0.662	-	0.607	0.715
N_2	-	28.33	-	-	30.12	-	-	33.21	-	-	38.45	-
λ_2	-	-	0.854	-	-	0.843	-	-	0.724	-	-	0.634
μ_2	-	-	0.692	-	-	0.708	-	-	0.747	-	-	0.812
n_2	-	-	0.247	-	-	0.259	-	-	0.262	-	-	0.395
J_2 ($\times10^{-3}$)	98	77	48	87	65	45	79	59	40	60	45	28

Figure 4 (see in Appendix) illustrates the dynamic responses of the test system for Poolco transactions using PI, PIDF, and FOI-TD controllers. The frequency deviation of area-1 (ΔF_1) versus time is shown in Figure 4(a), the frequency deviation of area-2 (ΔF_2) versus time is presented in Figure 4(b), and the tie-line power deviation between area-1 and area-2 (ΔP_{Tie12}) versus time is depicted in Figure 4(c). The maximum undershoot values and settling times corresponding to both frequency regulation and tie-line power control are summarized in Table 4. The comparative analysis clearly indicates that the FOI-TD controller provides superior performance compared to the conventional PI and PIDF controllers. Specifically, it achieves smaller peak deviations, reduced oscillatory behavior, and faster settling characteristics, thereby demonstrating enhanced capability in damping system oscillations. Consequently, the FOI-TD controller is identified as a highly effective secondary control strategy for AGC in interconnected power systems. The simulation model also accounts for the effect of integrating SIB units. In the test setup, the SIB gain is set to K_{SIB}=2.587, which corresponds with governor speed regulation coefficient of R=2.4 Hz/p.u.MW and a time constant T_{SIB}=0.01 s. The controller parameters and gains of the proposed FOI-TD scheme are optimally adjusted using the MFO algorithm.

Table 4. Dynamic output performancesof test system using proposed controllers for Poolco transactions

Controllers	Setting time			Peak over/under shoot (-ve)		
	ΔF_1 (sec)	ΔF_2 (sec)	ΔP_{Tie12} (sec)	ΔF_1 (Hz)	ΔF_2 (Hz)	ΔP_{Tie12} (p.u.MW)
PI	29.67	27.14	37.24	0.5921	0.3979	0.1451
PIDF	25.25	22.58	32.86	0.4144	0.2625	0.0937
FOI-TD	21.75	20.68	25.55	0.2951	0.1874	0.0649
FOI-TD with SIB unit	17.61	16.67	19.98	0.2071	0.1199	0.0423

Figure 5 presents the dynamic response of the test system with and without the inclusion of SIB units under FOI-TD control. The frequency deviation of area-1 (ΔF_1) is illustrated in Figure 5(a), while the frequency deviation of area-2 (ΔF_2) is shown in Figure 5(b). The corresponding tie-line power deviation between area-1 and area-2 (ΔP_{Tie12}) is depicted in Figure 5(c). These responses clearly demonstrate the enhanced transient stability and improved damping performance achieved through the optimized FOI-TD controller with SIB integration. The quantitative performance indices, including maximum undershoot and settling time for frequency deviations in both area control and tie-line power control, are summarized in Table 4. A comparative analysis of Figure 5 and Table 4 reveals that the incorporation of SIB units significantly improves system performance by reducing frequency and tie-line power deviations.

Consequently, the steady-state stability and overall dynamic behavior of the test system are substantially enhanced.

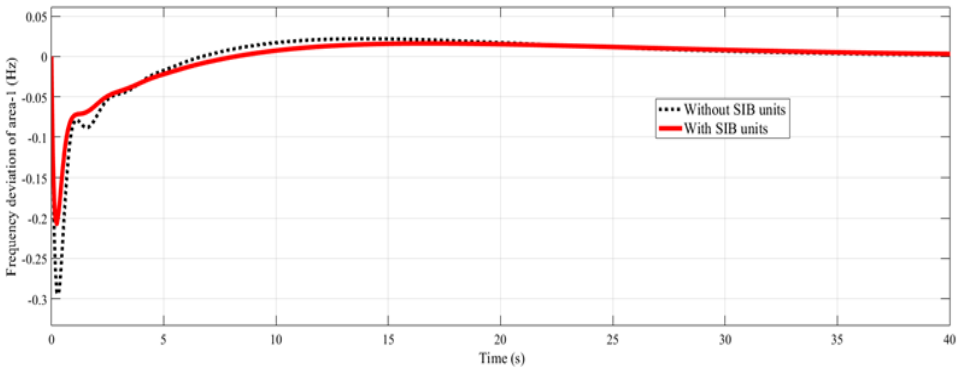

(a)

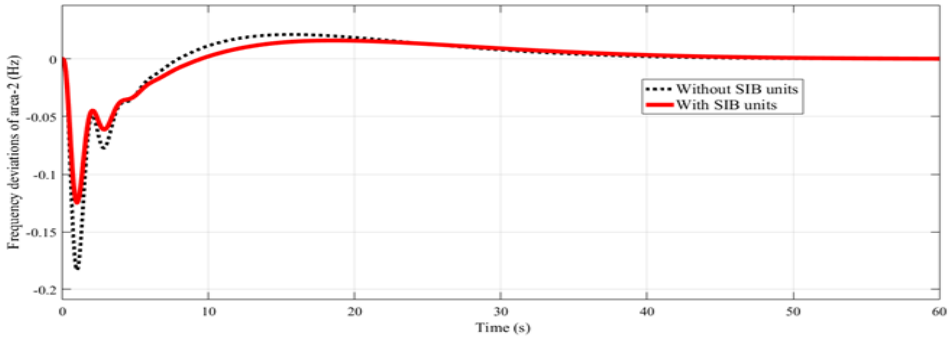

(b)

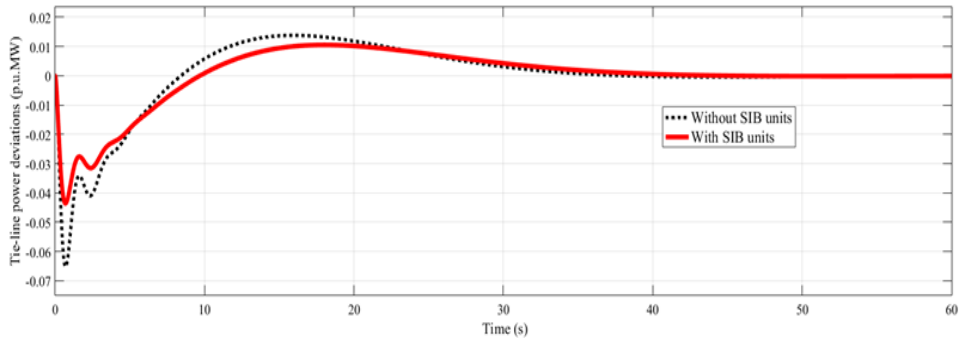

(c)

Figure 5. Dynamic response of test system for Poolco transactions with and without the inclusion of SIB units under FOI-TD control; (a) ΔF_1 vs. time, (b) ΔF_2 vs. time, and (c) ΔP_{Tie12} vs. time

3.2. Scenario 2: bilateral transactions

In this type of exchange, each Disco interacts directly with one or more Gencos simultaneously. Consequently, the relationships described in (15) must be applied. In the current situation, each Disco requests 0.1 p.u.MW from the Gencos, as specified by the CPF in the DPM.

$$DPM_2 = \begin{bmatrix} 0.2 & 0.3 & 0.1 & 0.4 \\ 0.3 & 0.2 & 0.3 & 0.1 \\ 0.25 & 0.1 & 0.25 & 0.3 \\ 0.25 & 0.4 & 0.35 & 0.2 \end{bmatrix} \quad (16)$$

The cost function values and control parameter settings for the proposed controllers, optimized using various algorithms, are summarized in Table 5. The outputs clearly shows that the given controllers

tuned with the MFO algorithm yield significantly lower cost function values compared to those optimized by PSO, BAT, and ALO techniques. The transient behavior of test system using different controllers is illustrated in Figure 6 (see in Appendix). The frequency deviation of area-1 (ΔF_1) versus time is shown in Figure 6(a), the frequency deviation of area-2 (ΔF_2) versus time is presented in Figure 6(b), the tie-line power deviation between area-1 and area-2 (ΔP_{Tie12}) versus time is depicted in Figure 6(c), and the tie-line power deviation error between area-1 and area-2 ($\Delta P_{Tie12\ error}$) versus time is shown in Figure 6(d). Detailed information on the peak overshoot, undershoot, and settling times association with area frequency deviations and tie-line power fluctuations for PI, PIDF, and FOI-TD controllers is provided in Table 6. Both Figure 6 and Table 6 demonstrate that the MFO-optimized FOI-TD controller achieves a substantial reduction in overshoot and undershoot while improving settling time when matched with the MFO-tuned PI and PIDF controllers.

Table 5. Control parameters of test system using PI, PIDF, and FOI-TD controllers for bilateral transactions

Control parameters	PSO			BAT			ALO			MFO		
	PI	PIDF	FOI-TD	PI	PIDF	FOI-TD	PI	PIDF	FOI-TD	PI	PIDF	FOI-TD
K_{P1}	0.311	0.298	0.274	0.307	0.291	0.269	0.295	0.282	0.275	0.271	0.264	0.252
K_{I1}	0.405	0.421	0.432	0.412	0.428	0.443	0.424	0.431	0.455	0.445	0.464	0.481
K_{D1}	-	0.614	0.692	-	0.628	0.697	-	0.641	0.705	-	0.673	0.731
N_1	-	20.78	-	-	22.87	-	-	25.78	-	-	28.45	-
λ_1	-	-	0.441	-	-	0.448	-	-	0.457	-	-	0.547
μ_1	-	-	0.417	-	-	0.434	-	-	0.447	-	-	0.598
n_1	-	-	0.578	-	-	0.581	-	-	0.593	-	-	0.678
J_1 ($\times 10^{-3}$)	123	114	96	118	104	86	106	96	77	81	75	54
K_{P2}	0.317	0.308	0.291	0.312	0.302	0.288	0.303	0.297	0.272	0.287	0.272	0.254
K_{I2}	0.435	0.452	0.498	0.447	0.461	0.508	0.459	0.473	0.511	0.494	0.508	0.537
K_{D2}	-	0.611	0.674	-	0.622	0.684	-	0.632	0.691	-	0.745	0.785
N_2	-	22.33	-	-	25.64	-	-	26.37	-	-	30.38	-
λ_2	-	-	0.552	-	-	0.598	-	-	0.608	-	-	0.624
μ_2	-	-	0.637	-	-	0.644	-	-	0.653	-	-	0.675
n_2	-	-	0.378	-	-	0.383	-	-	0.395	-	-	0.407
J_2($\times 10^{-3}$)	117	108	94	102	98	84	91	87	73	71	63	49

Table 6. Dynamic output performancesof test system using proposed controllers for bilateral transactions

Controllers	Setting time			Peak over/under shoot (-ve)		
	ΔF_1 (sec)	ΔF_2 (sec)	ΔP_{Tie12} (sec)	ΔF_1 (Hz)	ΔF_2 (Hz)	ΔP_{Tie12} (p.u MW)
PI	30.94	36.45	38.25	0.6204	0.3766	0.0848
PIDF	27.53	30.07	33.26	0.5548	0.3565	0.0627
FOI-TD	22.75	25.32	28.27	0.4042	0.3356	0.0423
FOI-TD with SIB unit	18.49	21.78	23.63	0.3736	0.3018	0.0235

The impact of integrating SIB units on the AGC loop is further investigated under varying uncontracted step load conditions using the MFO-optimized FOI-TD controller. Figure 7 presents the dynamic response of the test system for bilateral transactions with and without the inclusion of SIB units under FOI-TD control. The frequency deviation of area-1 (ΔF_1) versus time is shown in Figure 7(a), the frequency deviation of area-2 (ΔF_2) versus time is presented in Figure 7(b), the tie-line power deviation between area-1 and area-2 (ΔP_{Tie12}) versus time is depicted in Figure 7(c), and the tie-line power deviation error between area-1 and area-2 ($\Delta P_{Tie12\ error}$) versus time is shown in Figure 7(d). As indicated in Figure 7 and Table 6, the insertion of SIB units significantly enhances the system's dynamic performance. Their integration leads to faster settling times and considerable reductions in overshoot and undershoot for frequency variations and tie-line power oscillations under various load scenarios. Overall, the given control strategy demonstrates strong effectiveness in suppressing both inertia-mode and inter-area-mode oscillations, thereby improving the overall stability and transient performance of the power system when SIB units are deployed.

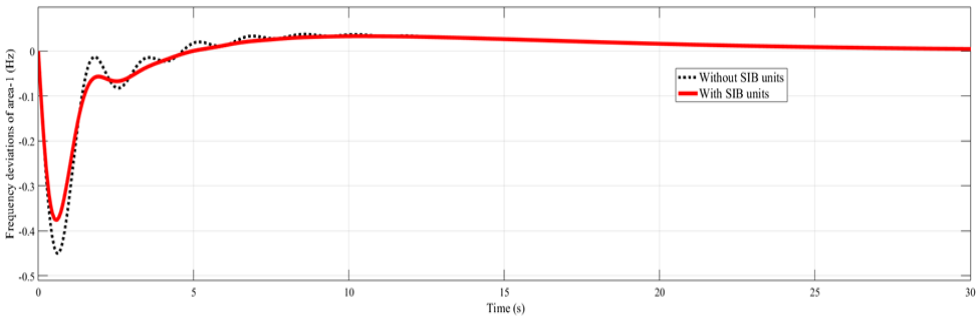

(a)

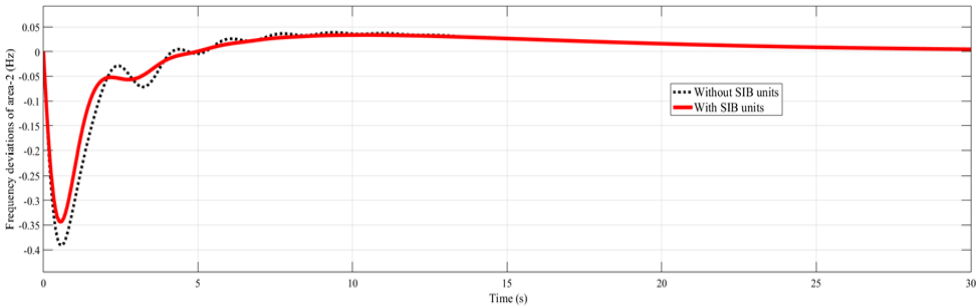

(b)

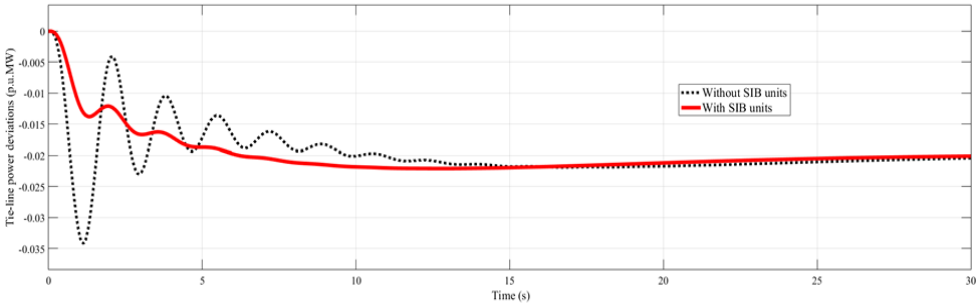

(c)

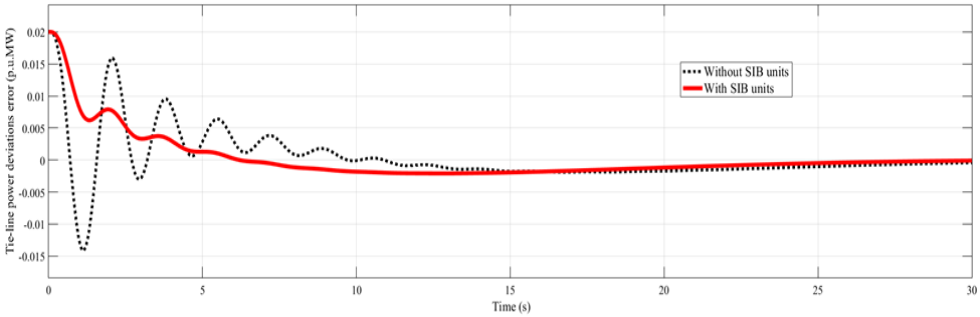

(d)

Figure 7. Dynamic response of test system for bilateral transactions with and without the inclusion of SIB units under FOI-TD control; (a) ΔF_1 vs. time, (b) ΔF_2 vs. time, (c) ΔP_{Tie12} vs. time, and (d) $\Delta P_{Tie12\ error}$ vs. time

4. CONCLUSION

This study focuses on the design and development of a FOI-TD controller for the AGC system of interconnected restructured power systems across two areas, which involve various possible transactions. The effectiveness of the FOI-TD controller is demonstrated in comparison to conventional PI and PIDF controllers. To optimize the control parameters and gain values of the proposed controllers, a recent

metaheuristic algorithm known as the MFO algorithm is utilized and compared with PSO, BAT, and ALO algorithms. The analysis of the simulated outcomes reveals that the MFO-tuned FOI-TD controller significantly reduces peak over/undershoot and improves settling time compared to the MFO-tuned PI and PIDF controllers. Furthermore, the MFO algorithm outperforms the others in terms of speed and produces lower cost function values (Ji) than the PSO, BAT, and ALO techniques. A notable advantage of the MFO-tuned FOI-TD controller is its adaptability, which enables it to effectively address the challenges of AGC. It provides robust management of parameter uncertainties, eliminates steady-state errors, and enhances overall system stability. Additionally, the integration of SIB units within the testing framework offers significant benefits by delivering quick and adaptive power responses to fluctuations in load demand. This further improves frequency regulation and enhances the reliability of the grid.

ACKNOWLEDGMENTS

The work in this manuscript did not receive any research funding/grant.

FUNDING INFORMATION

No research grant or contract was involved in this work.

AUTHOR CONTRIBUTIONS STATEMENT

This journal uses the Contributor Roles Taxonomy (CRediT) to recognize individual author contributions, reduce authorship disputes, and facilitate collaboration.

Name of Author	C	M	So	Va	Fo	I	R	D	O	E	Vi	Su	P	Fu
Nanthini B S	✓	✓	✓	✓	✓	✓	✓	✓	✓	✓	✓		✓	
Ilanji Akilandam Chidambaram		✓				✓	✓	✓	✓	✓	✓	✓		
Rajeswaran Sivasangari		✓	✓	✓		✓			✓	✓				

C : **C**onceptualization
M : **M**ethodology
So : **So**ftware
Va : **Va**lidation
Fo : **Fo**rmal analysis
I : **I**nvestigation
R : **R**esources
D : **D**ata Curation
O : Writing -**O**riginal Draft
E : Writing - Review &**E**diting
Vi : **Vi**sualization
Su : **Su**pervision
P : **P**roject administration
Fu : **Fu**nding acquisition

CONFLICT OF INTEREST STATEMENT

Authors state no conflict of interest

DATA AVAILABILITY

Data availability is not applicable to this paper as no new data were created or analyzed in this study.

REFERENCES

[1] M. M. Gulzar, D. Sibtain, M. Alqahtani, F. Alismail, and M. Khalid, "Load frequency control progress: A comprehensive review on recent development and challenges of modern power systems," *Energy Strategy Reviews*, vol. 57, p. 101604, Jan. 2025, doi: 10.1016/j.esr.2024.101604.

[2] M. T. Alrifai, M. F. Hassan, and M. Zribi, "Decentralized load frequency controller for a multi-area interconnected power system," *International Journal of Electrical Power and Energy Systems*, vol. 33, no. 2, pp. 198–209, Feb. 2011, doi: 10.1016/j.ijepes.2010.08.015.

[3] I. A. Khan, H. Mokhlis, N. N. Mansor, H. A. Illias, L. J. Awalin, and L. Wang, "New trends and future directions in load frequency control and flexible power system: A comprehensive review," *Alexandria Engineering Journal*, vol. 71, pp. 263–308, May 2023, doi: 10.1016/j.aej.2023.03.040.

[4] R. Patel, C. Li, L. Meegahapola, B. McGrath, and X. Yu, "Enhancing Optimal Automatic Generation Control in a Multi-Area Power System with Diverse Energy Resources," *IEEE Transactions on Power Systems*, vol. 34, no. 5, pp. 3465–3475, Sep. 2019, doi: 10.1109/TPWRS.2019.2907614.

[5] S. Debbarma, L. C. Saikia, and N. Sinha, "AGC of a multi-area thermal system under deregulated environment using a non-integer controller," *Electric Power Systems Research*, vol. 95, pp. 175–183, Feb. 2013, doi: 10.1016/j.epsr.2012.09.008.

[6] V. Donde, M. A. Pai, and I. A. Hiskens, "Simulation and optimization in an AGC system after deregulation," *IEEE Transactions on Power Systems*, vol. 16, no. 3, pp. 481–489, 2001, doi: 10.1109/59.932285.

[7] A. Pappachen and A. P. Fathima, "Critical research areas on load frequency control issues in a deregulated power system: A state-of-the-art-of-review," *Renewable and Sustainable Energy Reviews*, vol. 72, pp. 163–177, May 2017, doi: 10.1016/j.rser.2017.01.053.

[8] D. D. Rasolomampionona, M. Połecki, K. Zagrajek, W. Wróblewski, and M. Januszewski, "A Comprehensive Review of Load Frequency Control Technologies," *Energies*, vol. 17, no. 12, p. 2915, Jun. 2024, doi: 10.3390/en17122915.

[9] A. G-Marzbali, "Multi-area multi-source automatic generation control in deregulated power system," *Energy*, vol. 201, p. 117667, Jun. 2020, doi: 10.1016/j.energy.2020.117667.

[10] P. K. Hota and B. Mohanty, "Automatic generation control of multi source power generation under deregulated environment," *International Journal of Electrical Power and Energy Systems*, vol. 75, pp. 205–214, Feb. 2016, doi: 10.1016/j.ijepes.2015.09.003.

[11] K. Ullah, A. Basit, Z. Ullah, S. Aslam, and H. Herodotou, "Automatic generation control strategies in conventional and modern power systems: A comprehensive overview," *Energies*, vol. 14, no. 9, p. 2376, Apr. 2021, doi: 10.3390/en14092376.

[12] L. C. Saikia, J. Nanda, and S. Mishra, "Performance comparison of several classical controllers in AGC for multi-area interconnected thermal system," *International Journal of Electrical Power and Energy Systems*, vol. 33, no. 3, pp. 394–401, Mar. 2011, doi: 10.1016/j.ijepes.2010.08.036.

[13] G. M. Meseret, R. Kumhar, T. K. Mahato, P. Lakra, B. Kumari, and N. Kumar, "Design of Novel Secondary Controller for AGC in Multi-Area Multi-Sources Power System Incorporated Renewable Energy Using a Gray Wolf Optimizer Algorithm," *Engineering Reports*, vol. 7, no. 3, Mar. 2025, doi: 10.1002/eng2.70054.

[14] R. K. Sahu, S. Panda, and S. Padhan, "Optimal gravitational search algorithm for automatic generation control of interconnected power systems," *Ain Shams Engineering Journal*, vol. 5, no. 3, pp. 721–733, Sep. 2014, doi: 10.1016/j.asej.2014.02.004.

[15] S. Biswas, P. K. Roy, and K. Chatterjee, "FACTS-based 3DOF-PID Controller for LFC of Renewable Power System Under Deregulation Using GOA," *IETE Journal of Research*, vol. 69, no. 3, pp. 1486–1499, Apr. 2023, doi: 10.1080/03772063.2020.1870874.

[16] R. K.Sahu, S. Panda, A. Biswal, and G. T. C. Sekhar, "Design and analysis of tilt integral derivative controller with filter for load frequency control of multi-area interconnected power systems," *ISA Transactions*, vol. 61, pp. 251–264, Mar. 2016, doi: 10.1016/j.isatra.2015.12.001.

[17] N. Kumar, B. Tyagi, and V. Kumar, "Application of fractional order PID controller for AGC under deregulated environment," *International Journal of Automation and Computing*, vol. 15, no. 1, pp. 84–93, Feb. 2018, doi: 10.1007/s11633-016-1036-9.

[18] N. K. Jena, S. Sahoo, B. K. Sahu, and K. B. Mohanty, "Design of Fractional Order Cascaded Controller for AGC of a Deregulated Power System," *Journal of Control, Automation and Electrical Systems*, vol. 33, no. 5, pp. 1389–1417, 2022, doi: 10.1007/s40313-022-00897-z.

[19] S. Sahoo, N. K. Jena, P. K. Ray, and B. K. Sahu, "Selfish Herd Optimisation tuned fractional order cascaded controllers for AGC Analysis," *Soft Computing*, vol. 26, no. 6, pp. 2835–2853, Mar. 2022, doi: 10.1007/s00500-021-06518-2.

[20] B. Singh, A. Slowik, and S. K. Bishnoi, "Review on Soft Computing-Based Controllers for Frequency Regulation of Diverse Traditional, Hybrid, and Future Power Systems," *Energies*, vol. 16, no. 4, p. 1917, Feb. 2023, doi: 10.3390/en16041917.

[21] B. Hu, J. Cai, Z. Xing, P. Zhang, D. Wang, and K. A. Folly, "Control and optimization techniques for load frequency control of multi-area Cyber–Physical Power Systems: A literature review," *Annual Reviews in Control*, vol. 60, p. 101009, 2025, doi: 10.1016/j.arcontrol.2025.101009.

[22] R. Satheeshkumar and R. Shivakumar, "Ant Lion Optimization Approach for Load Frequency Control of Multi-Area Interconnected Power Systems," *Circuits and Systems*, vol. 07, no. 09, pp. 2357–2383, 2016, doi: 10.4236/cs.2016.79206.

[23] S. Mirjalili, "Moth-flame optimization algorithm: A novel nature-inspired heuristic paradigm," *Knowledge-Based Systems*, vol. 89, pp. 228–249, Nov. 2015, doi: 10.1016/j.knosys.2015.07.006.

[24] S. K. Sahoo *et al.*, "Moth Flame Optimization: Theory, Modifications, Hybridizations, and Applications," *Archives of Computational Methods in Engineering*, vol. 30, no. 1, pp. 391–426, Jan. 2023, doi: 10.1007/s11831-022-09801-z.

[25] H. Zamani, M. H. N-Shahraki, S. Mirjalili, F. S. Gharehchopogh, and D. Oliva, "A Critical Review of Moth-Flame Optimization Algorithm and Its Variants: Structural Reviewing, Performance Evaluation, and Statistical Analysis," *Archives of Computational Methods in Engineering*, vol. 31, no. 4, pp. 2177–2225, May 2024, doi: 10.1007/s11831-023-10037-8.

[26] S. A. Hosseini, M. Toulabi, A. A-Zadeh, and A. M. Ranjbar, "Battery energy storage systems and demand response applied to power system frequency control," *International Journal of Electrical Power and Energy Systems*, vol. 136, p. 107680, Mar. 2022, doi: 10.1016/j.ijepes.2021.107680.

[27] A. Oshnoei, M. Kheradmandi, and S. M. Muyeen, "Robust Control Scheme for Distributed Battery Energy Storage Systems in Load Frequency Control," *IEEE Transactions on Power Systems*, vol. 35, no. 6, pp. 4781–4791, Nov. 2020, doi: 10.1109/TPWRS.2020.2997950.

[28] Y. Cao, Q. Wu, C. Li, W. Jiao, and J. Tan, "Chance-constrained optimal sizing of BESS with emergency load shedding for frequency stability," *Applied Energy*, vol. 367, p. 123455, Aug. 2024, doi: 10.1016/j.apenergy.2024.123455.

[29] Y.Cao, "The opportunities and challenges of sodium ion battery," *Energy Storage Science and Technology*, vol. 9, no. 3, p. 757, 2020, doi: 10.19799/j.cnki.2095-4239.2020.0026.

[30] A. R. Nurohmah*et al.*, "Sodium-ion battery from sea salt: a review," *Materials for Renewable and Sustainable Energy*, vol. 11, no. 1, pp. 71–89, Apr. 2022, doi: 10.1007/s40243-022-00208-1.

[31] N. Aslfattahi*et al.*, "State-of-the-art review on electrolytes for sodium-ion batteries: Potential recent progress and technical challenges," *Journal of Energy Storage*, vol. 72, p. 108781, Nov. 2023, doi: 10.1016/j.est.2023.108781.

[32] T. Yu *et al.*, "The research and industrialization progress and prospects of sodium ion battery," *Journal of Alloys and Compounds*, vol. 958, p. 170486, Oct. 2023, doi: 10.1016/j.jallcom.2023.170486.

[33] I. A. Chidambaram and B. Paramasivam, "Optimized load-frequency simulation in restructured power system with Redox Flow Batteries and Interline Power Flow Controller," *International Journal of Electrical Power and Energy Systems*, vol. 50, no. 1, pp. 9–24, Sep. 2013, doi: 10.1016/j.ijepes.2013.02.004.

APPENDIX

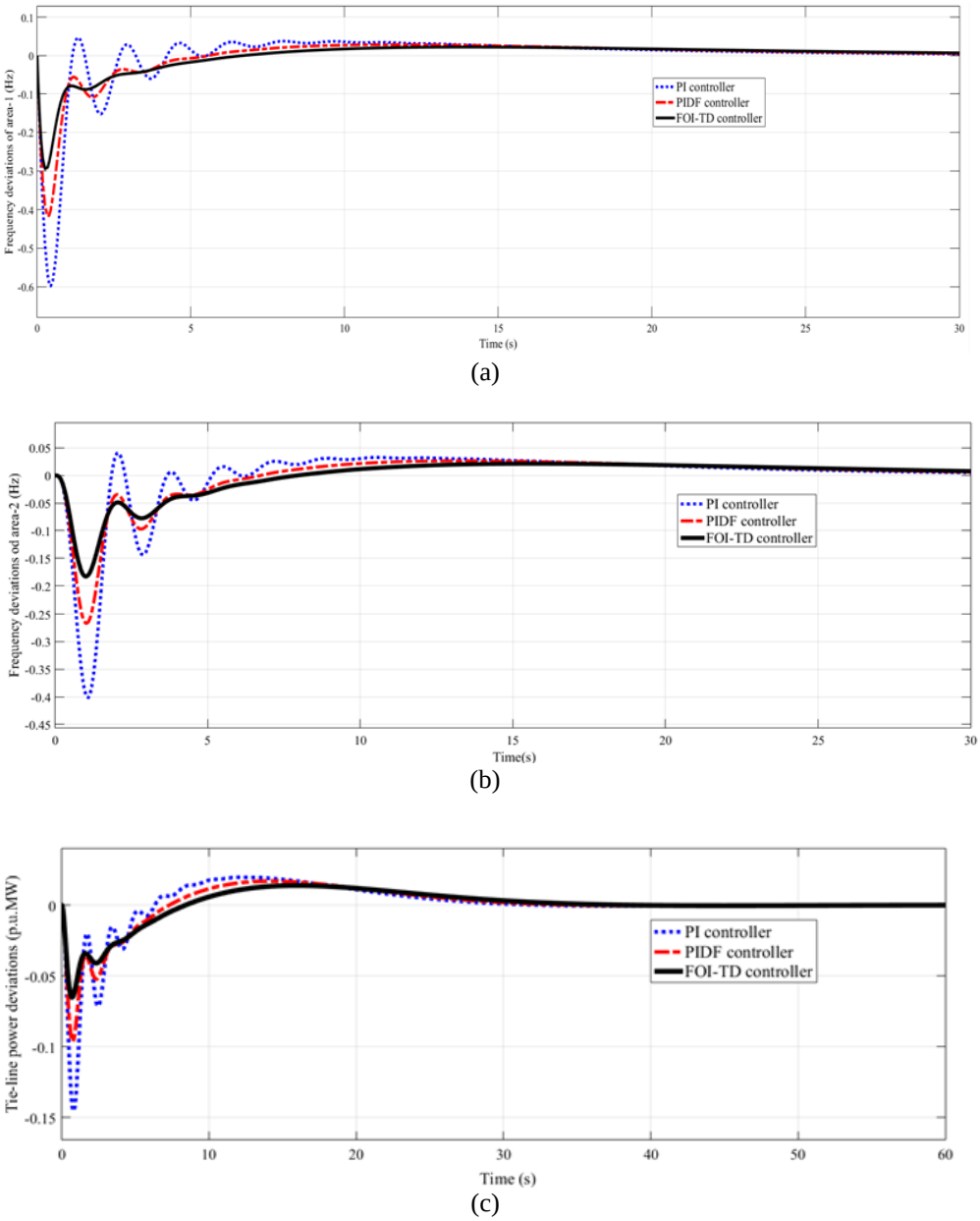

Figure 4. Dynamic respones of test system for Poolco transactions using PI, PIDF, and FOI-TD controllers; (a) ΔF_1 vs. time, (b) ΔF_2 vs. time, and (c) ΔP_{Tie12} vs. time

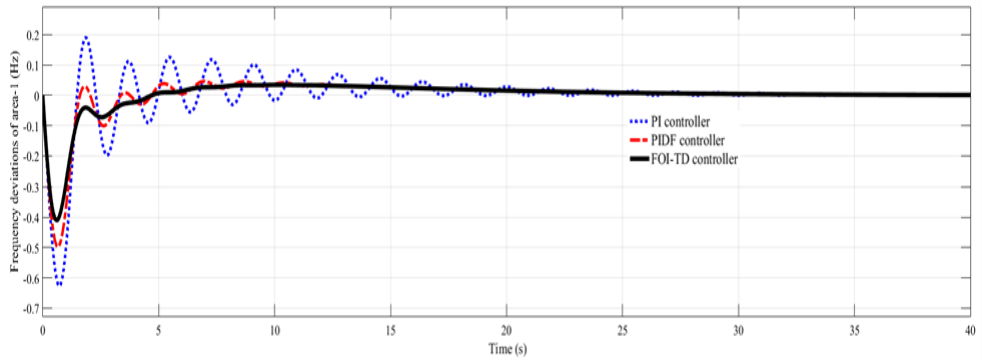

(a)

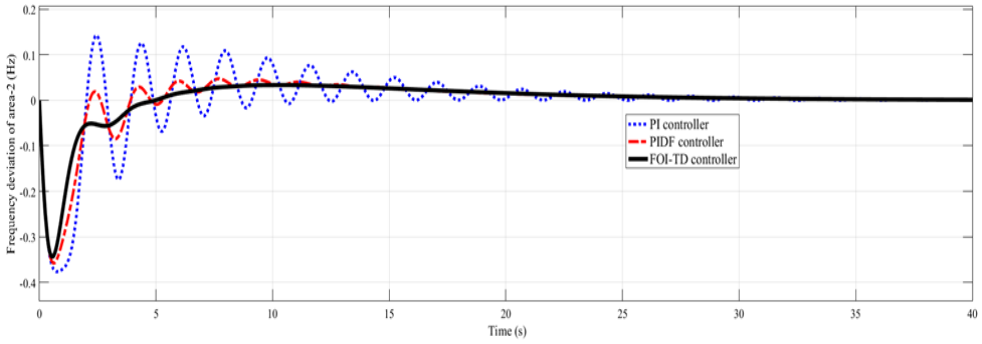

(b)

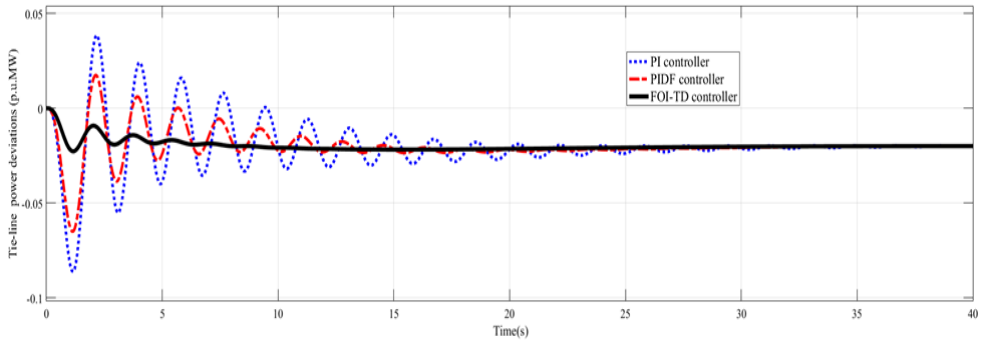

(c)

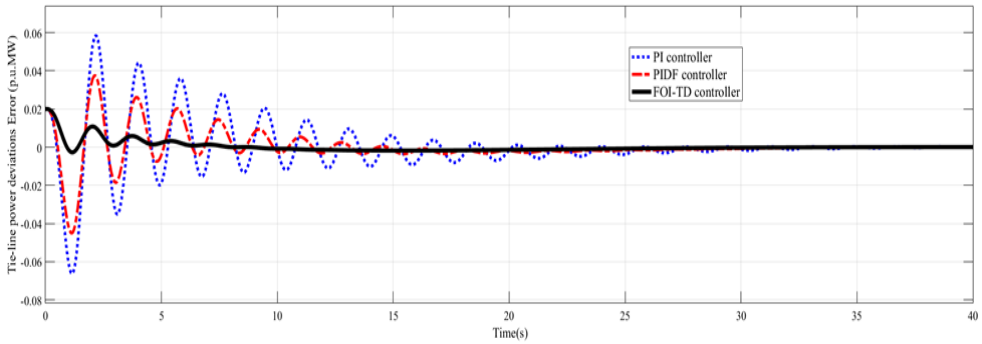

(d)

Figure 6. Dynamic respones of test system for bilateral transactions using PI, PIDF, and FOI-TD controllers; (a) ΔF_1 vs. time, (b) ΔF_2 vs. time, (c) ΔP_{Tie12} vs. time, and (d) $\Delta P_{Tie12\ error}$ vs. time

BIOGRAPHIES OF AUTHORS

Nanthini B S received the Bachelor of Engineering degree in Electrical Engineering from Annamalai University, Tamil Nadu, India, in 2018, and the Master's degree in Power Systems from Thiagarajar College of Engineering, Madurai, Tamil Nadu, India, in 2021. She is currently working as an Assistant Professor at Vels Institute of Science, Technology and Advanced Studies (VISTAS), Chennai, Tamil Nadu, India. She is presently pursuing the Ph.D. degree in Electrical and Electronics Engineering in the Department of Electrical Engineering, Annamalai University, Tamil Nadu, India. Her research interests include power system operation and control, solar energy systems, and electric vehicles. She can be contacted at email: nanthini.b.s.18@gmail.com.

Ilanji Akilandam Chidambaram received the Bachelor of Engineering degree in Electrical and Electronics Engineering in 1987, the Master of Engineering degree in Power System Engineering in 1992, and the Ph.D. degree in Electrical Engineering in 2007, all from Annamalai University, Annamalainagar, Tamil Nadu, India. During the period 1988–1993, he served as a Lecturer in the Department of Electrical Engineering, Annamalai University. Since 2007, he has been working as a professor, and since 2024, he has been serving as the head of the Department of Electrical Engineering, Annamalai University, Annamalainagar. He is a member of ISTE, ISC, and IET. His research interests include power system operation and control, control systems, power system restructuring, and smart grids. He has published 98 journal papers, supervised 14 Ph.D. research scholars, and authored a book. He can be contacted at email: driacdm@yahoo.com.

Rajeswaran Sivasangari received the Bachelor of Engineering degree in Electrical Engineering from the Government College of Engineering, Tirunelveli, Tamil Nadu, India, in 2000, and the Master's degree in Power Systems from Thiagarajar College of Engineering, Madurai, Tamil Nadu, India, in 2007. She obtained the Ph.D. degree in Electrical Engineering from Thiagarajar College of Engineering, Madurai, Tamil Nadu, India, in 2017. She is currently serving as professor and head at Sree Sowdambika College of Engineering, Aruppukottai, Tamil Nadu, India. Her research interests include power system protection, renewable energy technologies, electrical distribution networks, and battery technologies. She can be contacted at email: sivasangarianand@gmail.com.